

Quantum effects on the dispersion, threshold and gain characteristics of Brillouin scattered Stokes mode in ion-implanted semiconductor plasmas

PRAVESH¹, SUNITA DAHIYA¹, NAVNEET SINGH², MANJEET SINGH^{3,*}

¹Department of Physics, Baba Mastnath University, Asthal Bohar, Rohtak – 124021, India

²Department of Physics, Rajiv Gandhi Government College for Women, Bhiwani – 127021, India

³Department of Physics, Government College, Matanhail, Jhajjar – 124106, India

Quantum effects (QEs) in the dispersion, threshold, and gain characteristics of the Brillouin scattered Stokes mode (BSSM) in ion-implanted semiconductor plasmas are analytically investigated using coupled mode theory. Taking into account that the origin of stimulated Brillouin scattering lies in nonlinear induced polarisation of the medium, expressions are derived for complex effective Brillouin susceptibility (due to electrons and implanted colloids) and consequently the threshold pump amplitude and the gain constant of BSSM. Inclusion of QEs is done via quantum correction term in the hydrodynamic model of semiconductor plasmas. QEs modify the dispersion, threshold and gain characteristics of BSSM in ion implanted semiconductor plasmas. In contrast to the threshold and gain characteristics of BSSM, which are impacted only by electrons and are unaffected by implanted charged colloids, the Brillouin susceptibility caused by implanted colloids has a significant impact on the dispersion characteristics of BSSM. Finally, an extensive numerical study of the n- InSb/CO₂ laser system is performed for two different cases: (i) without QEs and (ii) with QEs. In both cases, the analysis offers two achievable resonances, at which the changes of sign as well as an enhancement of real part of effective Brillouin susceptibility and an enhancement of effective Brillouin gain constant are obtained. When QEs are included in the analysis, the entire spectrum shifts towards decreased levels of electron and colloidal carrier concentration.

(Received May 16, 2023; accepted October 6, 2023)

Keywords: Semiconductor quantum plasmas, Brillouin scattered Stokes mode, Quantum effects, Electron plasma wave, Implanted colloids, Electrons

1. Introduction

Stimulated Brillouin scattering (SBS) is a third-order nonlinear optical phenomenon that occurs when a pulsed (or CW) laser radiation interacts nonlinearly with an internally generated acoustic phonon mode in a Brillouin active medium. This interaction results in a significant amplification of the Stokes-shifted scattered mode, known as the Brillouin scattered Stokes mode (BSSM). SBS techniques have been used to enhance the performance of amplifiers, oscillators, pulse compressors etc. [1]. Because of its purity and high conversion efficiency, SBS is favoured among the numerous stimulated scattering techniques that result in optical phase conjugation (OPC) [2]. OPC-SBS may be considered a mechanism underlying the observed ray tracing backscatter in the process of laser-induced fusion [3]. Brillouin enhanced four-wave mixing (BEFWM), which combines SBS and FWM, has drawn a lot of attention because it can produce phase conjugate signals with incredibly high reflectivity [4]. The non-threshold conjugate reflection and amplification of weak pulses, as well as the operation of high power systems, have all been accomplished with BEFWM [5].

SBS has been studied in various media, including plasmas [1]. When it comes to developing optoelectronic components, semiconductor-plasmas have the most

potential among the wide range of Brillouin active media [6]. Additionally, in these media, large Brillouin nonlinearities are observed around the band gap resonant transition regimes [7]. SBS in semiconductor plasmas is currently a subject of many theoretical investigations [8-11]. SBS in semiconductor plasmas has been explored to enhance the Brillouin nonlinearity and consequently the gain of BSSM at low pump powers by proper selection of doping (free carriers) and simultaneous application of an external magnetic field [12, 13]. Apart from this, the Brillouin nonlinearity may be affected by implanted colloids concentration in ion-implanted semiconductor plasmas (IISPs).

The fabrication of semiconductor plasmas with regulated impurity profiles frequently uses the doping technique of ion implantation. However, because the implantation procedure damages the crystal lattice, post-implantation annealing is required to restore the lattice to a high degree and activate the dopants electrically [14]. The structural, electric, magnetic, (linear and nonlinear) optical properties of semiconductors can be modified by the implanted ions [15]. As a result, its primary use is in the development of semiconductor components. The depth profile of the implanted ion may be explained by chemical binding effects linked to ion-ion and ion-target atom interactions at low energies [16]. As a result of this

process, the implanted metal ions are neutralised during the slowing processes and eventually agglomerate to produce colloids of implanted materials.

The host material would display a variety of valuable thermodynamic, electrical, and optical properties that can be easily controlled, though, if the colloid particles could somehow be aligned in a long-range periodic fashion. Ion implantation is a popular method for creating diverse nanofabrication tools. The formation of tiny colloid particles in a long-range order lattice in magnetized and inhomogeneous semiconductor quantum plasmas has been studied theoretically [17, 18]. A stream of electrons with a drift speed similar to the ion-acoustic phonon speed in the crystal may be driven by the presence of an external drift field considerably below the breakdown of the semiconductor. By causing consistent electron current, these external fields can charge the growing colloid particles by sticky collisions. By using this method, colloidal plasma will be created, which resembles dusty plasma in that it contains electrons, negatively charged colloid particles, and vibrating positive lattice ion centres. This medium will become an IISP medium. In-depth research has been done on the function of charged colloids in IISPs for both identifying new modes of propagation and amplifying the waves of already existing modes [19, 20]. The existence of numerous novel modes and creative alterations to the characteristics of already-existing modes of propagation in IISPs has been demonstrated [21]. The most recent results further show that, even at frequencies where colloidal grains do not contribute to the linear motion of waves, the presence of charged colloids in IISPs has a significant impact on the wave properties of existing modes [22]. The colloids in these situations offer an immovable charge-neutralizing backdrop in IISPs.

Researchers have been concentrating their efforts on theoretical investigations of quantum effects (QEs) in plasmas for a long time. In super cooled plasmas, the de-Broglie wavelength connected to plasma particles approaches the Debye length [23]. It is possible to extend the magneto-hydrodynamic model of classical plasmas to encompass quantum plasmas; this newly created model is referred to as the quantum hydrodynamic (QHD) model [24]. In its most basic form, the QHD model is the generalisation of the classical hydrodynamic (CHD) model of plasmas with the inclusion of the quantum (Bohm potential) correction factor. Recently, this approach has been applied to the analytical study of QEs on parametric interactions [25], modulational interactions [26, 27], and SBS [28] in semiconductor magneto-plasmas.

For relatively large density of implanted colloids, QEs could become highly important in IISPs. The formation of colloid crystals in IISP has been reported by Zeba et al. [18]. Through the use of the Bohm potential, they have demonstrated that QEs on lattice electron-phonon coupling effects contribute to the dielectric response function of IISP. The present authors have recently investigated QEs on modulational amplification in IISPs [29]. In this investigation, we found that including QEs reduced the threshold pump amplitude and increased the growth rate of

the modulated beam for both the electrons and implanted colloids.

The gain coefficient of BSSM is an important parameter that characterizes SBS in the Brillouin medium. The dependence of gain coefficient of BSSM on a number of variables has created new opportunities for the deep understanding of SBS processes and the overall effectiveness of SBS-based nonlinear optical systems. The dependence of gain coefficient of BSSM on space, time, frequency, and line-width has been used to investigate [1]:

- (i) ultra-short amplification, pulse compression, and phase conjugation in a Brillouin cell;
- (ii) frequency comb, beam cleanup, coherent beam combination, fast and slow light in optical fibers;
- (iii) performance of fiber sensors, narrow line-width Brillouin lasers, and multi-wavelength fiber lasers; and
- (iv) performance of SBS spectrometer for material analysis.

It is anticipated that the dependence of gain coefficient of BSSM on the electron concentration and implanted colloid carrier concentration in IISPs will lead to new insights into laser-plasma interactions and the potential for the development of effective Brillouin amplifiers.

According to a literature review, QEs have not been investigated on SBS in IISPs. In the current paper, we conduct a theoretical formulation followed by a numerical analysis to examine the dispersion and gain characteristics of BSSM in IISPs under two different cases of interest, namely (i) the inclusion of QEs and (ii) the exclusion of QEs, keeping in mind the significant impact of QEs on SBS in IISPs. Expressions for the real and imaginary parts of the complex effective Brillouin susceptibility (caused by electrons and implanted colloids) are obtained using coupled mode theory of interacting waves and the assumption that the origin of SBS lies in finite nonlinear induced polarisation of IISPs. Through a real part of the complex effective Brillouin susceptibility, the dispersion characteristics of BSSM have been examined. The imaginary part of the complex effective Brillouin susceptibility is used to calculate the threshold pump amplitude and gain coefficient of BSSM. In order to enhance the amplification of BSSM at low pump amplitudes, efforts are made to optimise the concentration of electrons and implanted colloids as well as to set the value of the electron-plasma frequency and dust plasma frequency. Finally, an extensive numerical study is performed for n-InSb irradiated by a pulsed CO₂ laser.

The fact that implanted colloids, in addition to electrons, may significantly alter Brillouin nonlinearity and, as a result, the propagation characteristics of BSSM in IISPs, serves as the impetus for this investigation. This investigation becomes even more essential under high power pump irradiation since it helps to better understand SBS in IISPs. The gain characteristics of BSSM in IISPs have been modified in comparison to earlier studies of SBS in semiconductor magneto-plasmas using the QHD model [28], which makes this work a novel study with applications in the development of efficient Brillouin amplifiers and widely tunable Brillouin lasers.

2. Theoretical formulations

The theoretical formulation of the effective Brillouin susceptibility, the calculation of the threshold pump amplitude for SBS and the gain constant of the BSSM in IISP, including QEs, are covered in this section. Let a pump electric field $\vec{E}_0 = \hat{x}E_0 \exp[i(k_0x - \omega_0t)]$ be applied to IISP. In IISP, an intense pump (ω_0, \vec{k}_0) induces piezoelectric strain and derives an acoustic wave (ω_a, \vec{k}_a) . In turn, this acoustic wave serves as an induced density-modulated grating for the pump, resulting in the Brillouin scattered wave (ω_s, \vec{k}_s) . As a result, in IISP, the pump, acoustic, and scattered waves couple. Under pump irradiation, favourable circumstances lead to a large growth of both the induced acoustic wave and the Brillouin scattered wave, provided that the pump intensity must exceed a particular value, known as threshold intensity. Under dipole approximation, the non-uniformity of the pump field can be neglected [30].

In the present study of QEs on dispersion and gain characteristics of BSSM in IISPs, the incident pump wave is assumed to be linearly polarized. However, it may be assumed to be left/right handed circularly polarized, elliptically polarized, or hybrid. Using the same approach as presented here, the phenomenon of SBS has been studied in a semiconductor magneto-plasma under hydrodynamic approximation by assuming the propagation of a right-handed circularly polarized pump beam [31] and a hybrid pump beam [32]. It has been found that the polarization property of incident pump beam modifies the dispersion relations and consequently it affects the nonlinear absorption and refractive index of a semiconductor magneto-plasma.

The set of hydrodynamic (usually momentum transfer and continuity) equations that contain QEs via the Bohm-like potential are used to describe the carrier dynamics. Purely QEs are introduced by quantum statistics and the novel force associated with the quantum Bohm potential. Instead of dealing with the complexity of the Schrodinger-Poisson (2N equations), the QHD model is a simplified model that enables uncomplicated examination of the collective dynamics.

If IISP contains negatively charged colloids, the following is the requirement for charge neutrality:

$$n_{0i} = Z_{0d}n_{0d} + n_{0e}. \quad (1)$$

The number of unaffected charges that are present on the colloid grain is given by the symbol Z_{0d} (expressed in units of electronic charge). n_{0d} , n_{0e} and n_{0i} are the carrier densities of colloid grain, electrons, and unperturbed ions, respectively. The ultra-cold IISP acts like a Fermi gas and abides by the pressure law because, as IISP cools, the plasma carriers' de-Broglie wavelengths become equivalent to the system dimensions [33]. Eq. (2), which has been modified partly to take into account the Fermionic property of the colloids, is used in the model to incorporate quantum statistics.

$$P_{Fl} = \frac{m_l V_{Fl}^2 n_{l1}^3}{3n_{0l}^2} \quad (2)$$

In Eq. (2), P_{Fl} is the Fermi pressure, where the subscript $l = e, d$ stand for electrons and implanted colloids, respectively. n_{0l} and n_{l1} are unperturbed and perturbed electron densities, respectively. m_l is the mass of plasma carriers. $V_F (= 2k_B T_F / m)$ represents the Fermi speed, in which T_F is the Fermi temperature and k_B is the Boltzmann constant. The interpretation of pressure is based on the fluid's mean velocity being dispersed at different rates. The pressure term selected in this case is calculated under the assumption that electrons and colloids with homogeneous grain size are characterised by a zero temperature Fermi distribution function.

In IISP, the equation of generated acoustic wave is given by

$$\frac{\partial^2 u(x,t)}{\partial t^2} - \frac{C}{\rho} \frac{\partial^2 u(x,t)}{\partial x^2} + 2\Gamma_a \frac{\partial u(x,t)}{\partial t} = \frac{\beta}{\rho} \frac{\partial E_1}{\partial x} \quad (3)$$

where β is the piezoelectric constant, C is the elastic constant, ρ is the material density, Γ_a is the phenomenological damping parameter of the acoustic wave, and $u(x,t) = u \exp[i(k_a x - \omega_a t)]$ is the lattice displacement. The driving force per unit material density, which derives from the piezoelectric property of the medium, is the term on the right side of Eq. (3).

The term on right hand side of Eq. (3) is the driving force per unit material density having its origin in piezoelectric property of the medium.

In QHD model, the basic equations that describe SBS in IISP are as follows:

$$\frac{\partial v_{0l}}{\partial t} + v v_{0l} = -\frac{Z_l e}{m_l} E_0 \quad (4)$$

$$\frac{\partial v_{l1}}{\partial t} + v v_{l1} + \left(v_{0l} \cdot \frac{\partial}{\partial x} \right) v_{l1}$$

$$= -\frac{Z_l e}{m_l} E_s - \frac{1}{m_l n_0} \frac{\partial P}{\partial x} + \frac{\hbar^2}{4m_l^2 n_0} \frac{\partial^3 n_{ll}}{\partial x^3} \quad (5)$$

$$v_{0l} \frac{\partial n_{ll}}{\partial x} + n_{0l} \frac{\partial v_{ll}}{\partial x} = -\frac{\partial n_{ll}}{\partial t} \quad (6)$$

$$\frac{\partial E_1}{\partial x} + \frac{\beta}{\varepsilon} \frac{\partial^2 u}{\partial x^2} = -\frac{Z_l e n_{ll}}{\varepsilon} \quad (7)$$

Eqs. (4) and (5) are the momentum balance equations impacted by pump (E_0) and scattered (E_s) fields; v_{0l} and v_{ll} are the 0th and 1st order oscillatory fluid velocities of carriers. Here $Z_l e$ is the charge and v the momentum transfer collision frequency of carriers. The ratio of negative charges q_d present over the colloidal grains to the charge e may be used to characterise the charge state of carriers $Z_l (= q_l / e)$. Eq. (6) represents the continuity equation for carriers, where n_{ll} and n_{0l} are the perturbed and equilibrium carrier densities, respectively. The Poisson's equation [Eq. (7)] can be used to calculate the strong space charge field E_1 that was created as a result of charge carriers migration under the effect of the pump field. $\varepsilon = \varepsilon_0 \varepsilon_1$ is the dielectric permittivity, in which ε_0 and ε_1 being the free space permittivity and lattice dielectric constant of IISP, respectively.

The carrier density perturbation that results from the interaction of the pump wave and generated acoustic wave leads to the electron plasma wave (EPW) and generates nonlinear current density in IISP. Using Eqs. (2) to (7) and assuming $n_{la} \propto \exp[i(k_a x - \omega_a t)]$ and $n_0, v_0 \propto \exp[i(k_0 x - \omega_0 t)]$, we obtain

$$\begin{aligned} \frac{\partial^2 n_{ll}}{\partial t^2} + (\omega_{pl}^2 + k^2 V_{Fl}^2) n_{ll} + v \frac{\partial n_{le}}{\partial t} + \frac{Z_l e n_{0l} \beta}{m_l \varepsilon} \frac{\partial^2 u}{\partial x^2} \\ = -\bar{E}_l \frac{\partial n_{ll}}{\partial x} \end{aligned} \quad (8)$$

with $\bar{E}_l = -\left(\frac{Z_l e}{m_l} E_0\right)$, $V_{Fl}^2 = V_{Fl} (1 + \gamma_{el})^{1/2}$, and

$\gamma_{el} = \frac{\hbar^2 k^2}{8m_l k_B T_{Fl}}$ and $\omega_{pl} = \left(\frac{(Z_l)^2 n_{0l} e^2}{m_l \varepsilon}\right)^{1/2}$ is the plasma

frequency of carriers.

In obtaining Eq. (8), the Doppler shift has been disregarded under the assumption: $\omega_0 \gg v \gg k v_0$.¹⁰

The generation of one induced acoustic and one Brillouin scattered photon at the same time as the annihilation of one pump photon, is another way to define SBS. By this prospective, the transfer of energy among the pump, the induced acoustic, and the Brillouin scattered waves may be described by the following momentum and energy conservation relations: $\hbar k_0 = \hbar k_a + \hbar k_s$ and

$\hbar \omega_0 = \hbar \omega_a + \hbar \omega_s$. The Brillouin shift is determined by these equations, which are also referred to as the phase matching requirements. We can only take into account the resonant Stokes component ($\omega_s = \omega_0 - \omega_a, k_s = k_0 - k_a$) and disregard the higher-order components that are off-resonant by assuming that the interacting waves have a long interaction path [34]. We define the 1st order resonant Stokes component of Brillouin scattered wave as ‘‘Brillouin scattered Stokes mode’’ (BSSM). It is possible to distinguish between the fast (n_{fl}) and slow (n_{sl}) components of the perturbed carrier density (n_{ll}) induced in IISP, i.e. $n_{ll} = n_{fl} + n_{sl}$. The fast component $n_{fl} (\propto \exp[i(k_s x - \omega_s t)])$ corresponds to BSSM whereas; the slow component $n_{sl} (\propto \exp[i(k_a x - \omega_a t)])$ is associated with the induced acoustic wave. By resolving Eq. (8) into fast and slow components of perturbed carrier density, we obtain the following coupled equations:

$$\frac{\partial^2 n_{fl}}{\partial t^2} + v \frac{\partial n_{fe}}{\partial t} + (\omega_{pl}^2 + k^2 V_{Fl}^2) n_{fl} = -\bar{E}_l \frac{\partial n_{sl}^*}{\partial x} \quad (9a)$$

$$\begin{aligned} \frac{\partial^2 n_{sl}}{\partial t^2} + v \frac{\partial n_{se}}{\partial t} + (\omega_{pl}^2 + k^2 V_{Fl}^2) n_{sl} + \frac{Z_l e n_{0l} \beta}{m_l \varepsilon} \frac{\partial^2 u}{\partial x^2} \\ = -\bar{E}_l \frac{\partial n_{fl}^*}{\partial x} \end{aligned} \quad (9b)$$

The fast and slow components of the perturbed carrier density are denoted by the subscripts f and s , respectively. Indicators with an asterisk (*) represent the quantity's complex conjugate.

Eqs. (9a) and (9b) demonstrate how n_{fl} and n_{sl} are connected to one another by a pump electric field E_0 (via \bar{E}_l). In IISP, the plasma carriers, viz. electrons and charged colloids contribute to the Brillouin susceptibility. In order to avoid the complexities in the formulation of Brillouin susceptibility, distinct formulations have been established for the electrons and the implanted colloids.

2.1. Brillouin susceptibility due to electrons

For electrons, the slow component (n_{se}) of perturbed carrier density, including QEs, may be obtained from Eqs. (9a) and (9b) as:

$$\begin{aligned} n_{se} = \frac{-i\beta^2 e n_{0e} Z_e k^3 E_s^*}{\varepsilon \rho m_e (\omega_a^2 - k^2 V_a^2 - 2i\Gamma_a \omega_a)} \\ \times \left[\frac{k^2 |\bar{E}_e|^2}{(\delta_1^2 - i v \omega_a) - (\delta_2^2 + i v \omega_s)} \right]^{-1} \end{aligned} \quad (10)$$

where $\delta_1^2 = (\omega_{pe}^2 - \omega_a^2) + k^2 V_{Fe}^2$,

$\delta_2^2 = (\omega_{pe}^2 - \omega_s^2) + k^2 V_{Fe}^2$,

and

$$\omega_{pe} = \left(\frac{n_{0e} e^2}{m_e \varepsilon} \right)^{1/2} \text{ is electron plasma frequency.}$$

The induced current density (J_e) arising due to perturbations in electron concentration (at ω_s), including QEs, may be obtained from the relation

$$J_e(\omega_s) = -n_{se}^* Z_e e v_{0e}, \quad (11)$$

which yields

$$J_e(\omega_s) = \frac{i \varepsilon e Z_e A k \omega_{pe}^2 |E_0|^2 E_s^*}{2 m_e \Gamma_a \omega_0 \omega_a} \times \left[(\delta_1^2 - i v \omega_a) - \frac{k^2 |\bar{E}_e|^2}{(\delta_2^2 + i v \omega_s)} \right]^{-1} \quad (12)$$

where $A = \kappa^2 k^2 v_a^2$, $\kappa^2 = \frac{\beta^2}{\varepsilon C}$, $\omega_s = \omega_0 - \omega_a$,

$$v_{0e} = \frac{\bar{E}_e}{(v - i \omega_0)}.$$

In deriving Eq. (12), the oscillatory electron fluid velocity v_{0e} is obtained from Eq. (4).

The time integral of the induced current density can be used to express induced polarisation. Thus, the induced polarisation (P_e) due to electrons (at ω_s), including QEs, may be obtained from Eq. (12) as:

$$P_e(\omega_s) = \frac{\varepsilon e A k Z_e \omega_{pe}^2 |E_0|^2 E_s^*}{2 m_e \Gamma_a \omega_a \omega_0 \omega_s} \left[(\delta_1^2 - i v \omega_a) - \frac{k^2 |\bar{E}_e|^2}{(\delta_2^2 + i v \omega_s)} \right]^{-1} = \varepsilon_0 \chi_{Be} |E_0|^2 E_s^* \quad (13)$$

From Eq. (13), the Brillouin susceptibility (χ_{Be}) of IISP due to electrons, including QEs, may be obtained as:

$$\chi_{Be} = \frac{\varepsilon_1 e A k Z_e \omega_{pe}^2}{2 m_e \Gamma_a \omega_a \omega_0 \omega_s} \left((\delta_1^2 - i v \omega_a) - \frac{k^2 |\bar{E}_e|^2}{(\delta_2^2 + i v \omega_s)} \right)^{-1} \quad (14)$$

2.2. Brillouin susceptibility due to implanted colloids

The colloidal grains have a tendency to cling together and develop a net negative charge due to the high mobility of drifting electrons. For implanted colloids, the slow component (n_{sd}) of perturbed carrier density, including QEs, may be obtained from Eqs. (7) and (9) as:

$$n_{sd}^* = \frac{-i \beta^2 e n_{0d} Z_d k^3 E_s^*}{\varepsilon \rho m_d (\omega_a^2 - k^2 v_a^2 - 2i \Gamma_a \omega_s)} \times \left[(\Delta^2 - \omega_a^2) - \frac{k^2 |\bar{E}_d|^2}{(\Delta^2 - \omega_s^2)} \right]^{-1} \quad (15)$$

where $\Delta^2 = \omega_{pd}^2 + k^2 V_{Fd}^2$, in which

$$\omega_{pd} = \left(\frac{(Z_d)^2 n_{0d} e^2}{m_d \varepsilon} \right)^{1/2} \text{ is dust plasma frequency.}$$

The induced current density (J_d) arising due to perturbations in colloid concentration (at ω_s), including QEs, may be obtained from the relation

$$J_d(\omega_s) = -n_{sd}^* Z_d e v_{0d} \quad (16)$$

which yields

$$J_d(\omega_s) = \frac{i \varepsilon e Z_d A k \omega_{pd}^2 |E_0|^2 E_s^*}{2 m_d \Gamma_a \omega_a \omega_0} \times \left[(\Delta^2 - \omega_a^2) - \frac{k^2 |\bar{E}_d|^2}{(\Delta^2 - \omega_s^2)} \right]^{-1} \quad (17)$$

where $A = \kappa^2 k^2 v_a^2$, $\kappa^2 = \frac{\beta^2}{\varepsilon C}$, $\omega_s = \omega_0 - \omega_a$, and

$$v_{0d} = \frac{\bar{E}_d}{(-i \omega_0)}.$$

The time integral of the induced current density can be used to express induced polarisation. Thus, the induced polarisation (P_d) due to implanted colloids (at ω_s), including QEs, may be obtained from Eq. (17) as:

$$P_d(\omega_s) = \frac{\varepsilon e A k Z_d \omega_{pd}^2 |E_0|^2 E_s^*}{2 m_d \Gamma_a \omega_a \omega_0 \omega_s} \left((\Delta^2 - \omega_a^2) - \frac{k^2 |\bar{E}_d|^2}{(\Delta^2 - \omega_s^2)} \right)^{-1} = \varepsilon_0 \chi_{Bd} |E_0|^2 E_s^* \quad (18)$$

From Eq. (18), the Brillouin susceptibility (χ_{Bd}) of IISP due to implanted colloids, including QEs, may be obtained as:

$$\chi_{Bd} = \frac{\varepsilon_1 e A k Z_d \omega_{pd}^2}{2 m_d \Gamma_a \omega_a \omega_0 \omega_s} \left((\Delta^2 - \omega_a^2) - \frac{k^2 |\bar{E}_d|^2}{(\Delta^2 - \omega_s^2)} \right)^{-1} \quad (19)$$

2.3. Effective Brillouin susceptibility of medium

The effective Brillouin susceptibility ($\chi_B^{(e)}$) of IISP, including QEs, is the sum of Brillouin susceptibilities due to electrons (χ_{Be}) and due to implanted colloids (χ_{Bd}). Addition of Eqs. (14) and (19) yields

$$\chi_B^{(e)} = \chi_{Be} + \chi_{Bd} = \frac{\varepsilon_1 e A k}{2\Gamma_a \omega_a \omega_0 \omega_s} \times \left[\frac{Z_e \omega_{pe}^2}{m_e} \left((\delta_1^2 - i\nu\omega_a) - \frac{k^2 |\bar{E}_e|^2}{(\delta_2^2 + i\nu\omega_s)} \right)^{-1} + \frac{Z_d \omega_{pd}^2}{m_d} \left((\Delta^2 - \omega_a^2) - \frac{k^2 |\bar{E}_d|^2}{(\Delta^2 - \omega_s^2)} \right)^{-1} \right] \quad (20)$$

Eq. (20) demonstrates that $\chi_B^{(e)}$ is a complex quantity, and it can be written as: $\chi_B^{(e)} = \text{Re}(\chi_B^{(e)}) + i \text{Im}(\chi_B^{(e)})$, where $\text{Re}(\chi_B^{(e)})$ and $\text{Im}(\chi_B^{(e)})$ stand for the real and imaginary parts of $\chi_B^{(e)}$, respectively. Rationalization of Eq. (20) yields:

$$\begin{aligned} \text{Re}(\chi_B^{(e)}) &= \text{Re}(\chi_{Be}) + \text{Re}(\chi_{Bd}) \\ &= \frac{\varepsilon_1 A k}{2\Gamma_a \omega_a \omega_0 \omega_s} \\ &\times \left[\frac{Z_e e \omega_{pe}^2}{2m_e} \left(\frac{\delta_2^4 \delta_1^2 - \delta_2^2 k^2 |\bar{E}_e|^2 + \delta_1^2 \nu^2 \omega_s^2}{(\delta_1^2 \delta_2^2 + \nu^2 \omega_a \omega_s - k^2 |\bar{E}_e|^2)^2 + (\delta_2^2 \nu \omega_a - \delta_1^2 \nu \omega_s)^2} \right) \right. \\ &\quad \left. + \frac{Z_d e \omega_{pd}^2}{m_d} \left((\Delta^2 - \omega_a^2) - \frac{k^2 |\bar{E}_d|^2}{(\Delta^2 - \omega_s^2)} \right)^{-1} \right] \quad (21a) \\ \text{Im}(\chi_B^{(e)}) &= \text{Im}(\chi_{Be}) + \text{Im}(\chi_{Bd}) \\ &= \frac{\varepsilon_1 A k}{2\Gamma_a \omega_a \omega_0 \omega_s} \\ &\times \left[\frac{Z_e e \omega_{pe}^2}{2m_e} \left(\frac{\delta_2^4 \nu \omega_a + \nu^3 \omega_a \omega_s^2 - \nu \omega_s k^2 |\bar{E}_e|^2}{(\delta_1^2 \delta_2^2 + \nu^2 \omega_a \omega_s - k^2 |\bar{E}_e|^2)^2 + (\delta_2^2 \nu \omega_a - \delta_1^2 \nu \omega_s)^2} \right) \right] \quad (21b) \end{aligned}$$

It can be inferred from Eqs. (21a) and (21b) that both $\text{Re}(\chi_{Be})$ and $\text{Re}(\chi_{Bd})$ are finite, whereas $\text{Im}(\chi_{Be})$ is finite and $\text{Im}(\chi_{Bd}) = 0$. This means that while both electrons and implanted charged colloids contribute to the formulation of the real part of effective Brillouin susceptibility ($\text{Re}(\chi_B^{(e)})$), only electrons are responsible for the formulation of the imaginary part of effective Brillouin susceptibility ($\text{Im}(\chi_B^{(e)})$), which is unaffected by implanted charged colloids. The expressions for $\text{Re}(\chi_B^{(e)})$ and $\text{Im}(\chi_B^{(e)})$ of IISP, excluding QEs, can be obtained by putting $V_{Fe}' = 0$ (in δ_1 , δ_2 and Δ) in Eqs. (21a) and (21b), respectively. The dispersion of BSSM is well known to be caused by the real part of effective Brillouin susceptibility, whereas parametric gain/loss is caused by the imaginary part of effective Brillouin susceptibility. The quantum correction term (through δ_1 , δ_2 , and Δ)

effectively modifies the dispersion as well as the gain characteristics of BSSM in IISP.

2.4. Threshold pump amplitude

SBS is well known to happen at pump field amplitudes above a specific threshold, i.e. $E_0 > E_{0T}$. The condition $\text{Im}(\chi_B^{(e)}) = 0$ yields the pump amplitude, including QEs, which must be required for SBS to occur in IISP. This condition yields:

$$E_{0T} = \frac{m_e \omega_a}{Z_e e k \omega_s} (\delta_2^4 \omega_s + \nu^2 \omega_s^3)^{1/2} \quad (22)$$

The expression for E_{0T} , excluding QEs, can be obtained by putting $V_{Fe}' = 0$ (in δ_2) in Eq. (22). E_{0T} is significantly affected by the wave number magnitude k , electron concentration n_{0e} (via ω_{pe} in δ_2), and quantum correction term (via δ_2).

2.5 Effective gain constant of BSSM

At pump field amplitudes above the threshold ($E_0 > E_{0T}$), the effective gain constant of BSSM in IISP, including QEs, is given by [8]

$$g_B^{(e)} = \frac{k_s}{2\varepsilon_1} [\text{Im}(\chi_B^{(e)})] = \frac{\varepsilon_1 A k k_s Z_e e \omega_{pe}^2}{8\varepsilon_1 \Gamma_a \omega_a \omega_0 \omega_s m_e} \times \left(\frac{\delta_2^4 \nu \omega_a + \nu^3 \omega_a \omega_s^2 - \nu \omega_s k^2 |\bar{E}_e|^2}{(\delta_1^2 \delta_2^2 + \nu^2 \omega_a \omega_s - k^2 |\bar{E}_e|^2)^2 + (\delta_2^2 \nu \omega_a - \delta_1^2 \nu \omega_s)^2} \right) \quad (23)$$

The effective gain constant of BSSM in IISP, excluding QEs, can be obtained by putting $V_{Fe}' = 0$ (in δ_1 and δ_2) in Eq. (23). $g_B^{(e)}$ is significantly affected by the wave number magnitude k , electron concentration n_{0e} (via ω_{pe} in δ_2), pump field amplitude E_0 (via \bar{E}), and quantum correction term (via δ_1 and δ_2).

3. Results and discussion

We take into account an n-InSb crystal that has been properly illuminated by a pulsed 10.6 μm CO₂ laser for numerical analysis. The material parameters of the selected sample are given in Ref. [29, 35, 36]. The values of $\text{Re}(\chi_{Be})$, $\text{Re}(\chi_{Bd})$, $\text{Im}(\chi_{Be})$, $\text{Im}(\chi_{Bd})$, E_{0T} , and $g_B^{(e)}$ are determined under two categories, viz. excluding QEs and including QEs, and are shown in Table 1. The determined values of real and imaginary parts of Brillouin susceptibility due to electrons and due to implanted colloids are well in agreement with available literature using CHD model [11] and QHD model [28].

We observed that the plasma carrier concentration significantly affect the real and imaginary parts of effective Brillouin susceptibility and hence the threshold pump amplitude as well as the gain constant of BSSM for both the cases, viz. (i) excluding QEs (when $\omega_{pe}^2 \sim \omega_s^2$), and (ii) including QEs (when $\omega_{pe}^2 \sim \omega_s^2 + k^2 V_{Fe}^2$). Thus the

following ratios are obtained: $(E_{0T})_{QE} / E_{0T} = 0.73 \times 10^2$ and $(g_B^{(e)})_{QE} / g_B^{(e)} = 27.82$.

Table 1. Calculated values of $\text{Re}(\chi_{Be})$, $\text{Re}(\chi_{Bd})$, $\text{Im}(\chi_{Be})$, $\text{Im}(\chi_{Bd})$, E_{0T} , and $g_B^{(e)}$ around resonances $\omega_{pe}^2 \sim \omega_a^2$ and $\omega_{pe}^2 \sim \omega_s^2$ (when QEs are excluded), and $\omega_{pe}^2 \sim \omega_a^2 + k^2 V_{Fe}^2$ and $\omega_{pe}^2 \sim \omega_s^2 + k^2 V_{Fe}^2$ (when QEs are included)

Parameter		Symbol	Units	Calculated values			
				(Excluding QEs)		(Including QEs)	
				$\omega_{pe}^2 \sim \omega_a^2$	$\omega_{pe}^2 \sim \omega_s^2$	$\omega_{pe}^2 \sim \omega_a^2 + k^2 V_{Fe}^2$	$\omega_{pe}^2 \sim \omega_s^2 + k^2 V_{Fe}^2$
Real part of Brillouin susceptibility	for electrons	$\text{Re}(\chi_{Be})$	$\text{m}^2 \text{V}^{-2}$	$\pm 2.2 \times 10^{-18}$	$\pm 2.5 \times 10^{-17}$	$\pm 4.0 \times 10^{-18}$	$\pm 5.0 \times 10^{-17}$
	for colloids	$\text{Re}(\chi_{Bd})$	$\text{m}^2 \text{V}^{-2}$	$\pm 2.5 \times 10^{-18}$	$\pm 5.8 \times 10^{-18}$	$\pm 1.8 \times 10^{-17}$	$\pm 6.7 \times 10^{-17}$
Imaginary part of Brillouin susceptibility	for electrons	$\text{Im}(\chi_{Be})$	$\text{m}^2 \text{V}^{-2}$	$\pm 3.3 \times 10^{-18}$	$\pm 3.7 \times 10^{-17}$	$\pm 6.1 \times 10^{-18}$	$\pm 7.7 \times 10^{-17}$
	for colloids	$\text{Im}(\chi_{Bd})$	$\text{m}^2 \text{V}^{-2}$	$\pm 4.1 \times 10^{-18}$	$\pm 6.5 \times 10^{-18}$	$\pm 3.4 \times 10^{-17}$	$\pm 8.2 \times 10^{-17}$
Threshold pump amplitude		E_{0T}	V m^{-1}	-----	6.8×10^7	-----	1.5×10^6
Gain coefficient of BSSM		$g_B^{(e)}$	m^{-1}	7.8×10^2	2.3×10^3	1.1×10^4	6.4×10^4

3.1. Dispersion characteristics of BSSM

The nature of dependence of dispersion characteristics of BSSM originating via real part of effective Brillouin susceptibility, viz. $\text{Re}(\chi_B^{(e)})$ of IISP on different parameters such as wave number magnitude, electron concentration, implanted colloid concentration, and pump field amplitude can be studied from Eq. (21a). The results are displayed in Figs. (1) to (4).

Fig. 1 illustrates the relationship between the real part of effective Brillouin susceptibility $\text{Re}(\chi_B^{(e)})$ and wave number magnitude k for the cases: (i) excluding QEs, and (ii) including QEs.

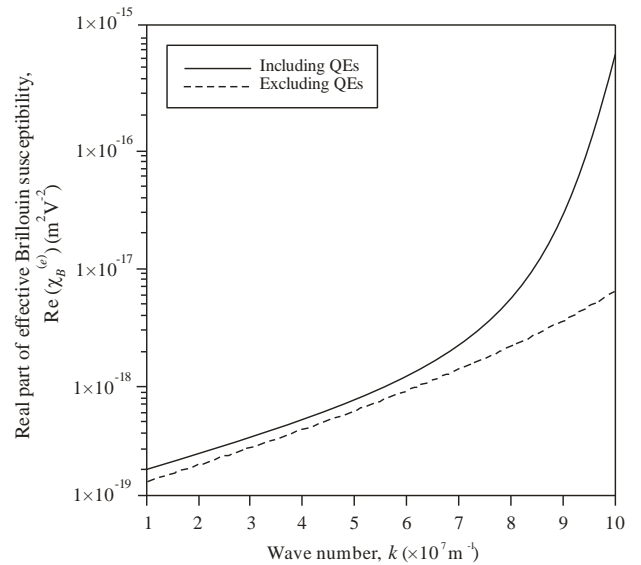


Fig. 1. Variation of real part of effective Brillouin susceptibility $\text{Re}(\chi_B^{(e)})$ with wave number magnitude k for the cases: (i) excluding QEs, and (ii) including QEs

For smaller magnitudes of wave number ($\sim 10^7 \text{ m}^{-1}$), in both the cases $\text{Re}(\chi_B^{(e)})$ is very small ($\sim 10^{-19} \text{ m}^2 \text{V}^{-2}$) and the curves are closer. When QEs are excluded, $\text{Re}(\chi_B^{(e)})$ increases linearly with increasing k throughout its plotted range. However, when QEs are taken into

account, $\text{Re}(\chi_B^{(e)})$ increases linearly with increasing wave number for $k \leq 6 \times 10^7 \text{ m}^{-1}$. Beyond this value of k , $\text{Re}(\chi_B^{(e)})$ exhibits parabolic variation with increasing k . A close look at the figure reveals that the curves in both cases are very close to one another for $k \leq 6 \times 10^7 \text{ m}^{-1}$, indicating that QEs on $\text{Re}(\chi_B^{(e)})$ are negligible in this regime of wave number and get separated for $k > 6 \times 10^7 \text{ m}^{-1}$, indicating that QEs on $\text{Re}(\chi_B^{(e)})$ are more pronounced in this regime of wave number. One way to describe this is as follows. When QEs are not taken into account ($V_{Fe}' = 0$), the terms δ_1^2 , δ_2^2 and Δ^2 become smaller and independent of k and their contribution become negligible resulting in the dependence $\text{Re}(\chi_B^{(e)}) \propto k$ [Eq. (21a)]. However, when QEs are taken into account ($V_{Fe}' \neq 0$), the terms δ_1^2 , δ_2^2 and Δ^2 containing wave number k dominate over other terms and hence $\text{Re}(\chi_B^{(e)})$ exhibits the complex dependence on k .

Fig. 2 shows how the real part of the effective Brillouin susceptibility $\text{Re}(\chi_B^{(e)})$ varies with electron concentration n_{0e} for the cases: (i) in which QEs are excluded and (ii) in which QEs are included. To draw this behaviour, we consider the contribution of n_{0e} to $\text{Re}(\chi_B^{(e)})$; the contribution of n_{0d} to $\text{Re}(\chi_B^{(e)})$ is neglected. Keeping in mind that IISPs can be doped by free carriers (electrons) over wide regime, we consider the wide range of electron concentration ($10^{19} \text{ m}^{-3} < n_{0e} < 10^{23} \text{ m}^{-3}$). This clearly shows the substantial enhancement of $\text{Re}(\chi_B^{(e)})$ as well as change of its sign. For clear understanding, the features corresponding to both the cases can be explained separately.

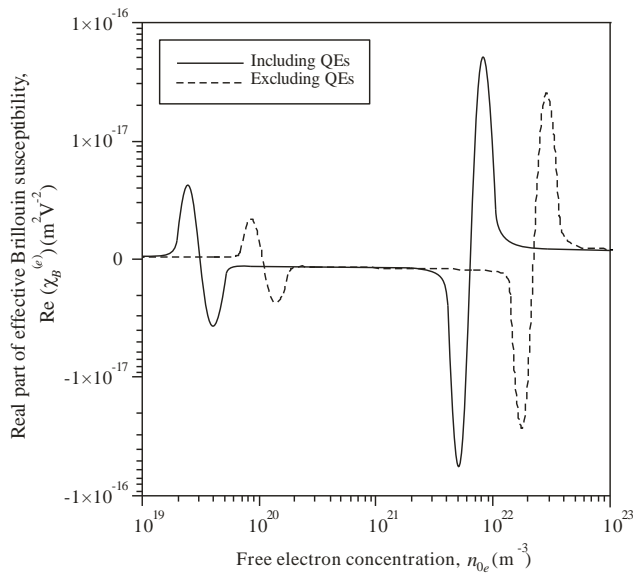


Fig. 2. Variation of real part of effective Brillouin susceptibility $\text{Re}(\chi_B^{(e)})$ with electron concentration n_{0e} for the cases: (i) excluding QEs, and (ii) including QEs

When QEs are not taken into account ($V_{Fe}' = 0$), $\text{Re}(\chi_B^{(e)})$ is positive, very small, and remain unaffected by the electron concentration for $n_{0e} \leq 6 \times 10^{19} \text{ m}^{-3}$. The regime $6 \times 10^{19} \text{ m}^{-3} < n_{0e} \leq 2 \times 10^{20} \text{ m}^{-3}$ is quite sensitive to the nature of the curve. In this regime, with increasing n_{0e} , $\text{Re}(\chi_B^{(e)})$ starts increasing, achieving a positive peak value ($2.2 \times 10^{-18} \text{ m}^2 \text{ V}^{-2}$) at $n_{0e} = 8 \times 10^{19} \text{ m}^{-3}$. Beyond this point, n_{0e} is only marginally increased, and $\text{Re}(\chi_B^{(e)})$ begins rapidly decreasing. At $n_{0e} = 1.1 \times 10^{20} \text{ m}^{-3}$, $\text{Re}(\chi_B^{(e)})$ vanishes. With further increasing n_{0e} beyond this value, $\text{Re}(\chi_B^{(e)})$ changes sign achieving a peak negative value ($-2.2 \times 10^{-18} \text{ m}^2 \text{ V}^{-2}$) at $n_{0e} = 1.5 \times 10^{20} \text{ m}^{-3}$. For $1.5 \times 10^{20} \text{ m}^{-3} \leq n_{0e} \leq 2 \times 10^{20} \text{ m}^{-3}$, $\text{Re}(\chi_B^{(e)})$ increases sharply but remains negative and vanishingly small up to $n_{0e} < 1.2 \times 10^{22} \text{ m}^{-3}$. The nature of curve of $\text{Re}(\chi_B^{(e)})$ versus n_{0e} is repeated again in the regime $1.2 \times 10^{22} \text{ m}^{-3} \leq n_{0e} \leq 5 \times 10^{22} \text{ m}^{-3}$ like the regime $6 \times 10^{19} \text{ m}^{-3} < n_{0e} \leq 2 \times 10^{20} \text{ m}^{-3}$. For $n_{0e} > 2 \times 10^{20} \text{ m}^{-3}$, $\text{Re}(\chi_B^{(e)})$ continues to be positive and vanishingly small. The behaviour of $\text{Re}(\chi_B^{(e)})$ in the domain $1.5 \times 10^{20} \text{ m}^{-3} \leq n_{0e} \leq 2 \times 10^{20} \text{ m}^{-3}$ is caused by resonance between the frequencies of the EPW and the acoustic wave, i.e. $\omega_{pe}^2 \sim \omega_a^2$ (via δ_1^2) while the behaviour of $\text{Re}(\chi_B^{(e)})$ in the domain $1.2 \times 10^{22} \text{ m}^{-3} \leq n_{0e} \leq 5 \times 10^{22} \text{ m}^{-3}$ is caused by resonance between frequencies of EPW and BSSM, i.e. $\omega_{pe}^2 \sim \omega_s^2$ (via δ_2^2).

When QEs are taken into account ($V_{Fe}' \neq 0$), the entire spectrum has been shifted towards smaller values of electron concentration and the peak (negative and positive) values of $\text{Re}(\chi_B^{(e)})$ have been enhanced significantly. The change of sign of $\text{Re}(\chi_B^{(e)})$ previously occurred at $n_{0e} = 1.1 \times 10^{20}$, and $1.2 \times 10^{22} \text{ m}^{-3}$, have now been shifted to $n_{0e} = 2 \times 10^{19}$, and $6 \times 10^{21} \text{ m}^{-3}$, respectively. This change occurred due to inclusion of QEs via appearance of the term $k^2 V_{Fe}'^2$ in δ_1^2 and δ_2^2 . In this case, the change of sign of $\text{Re}(\chi_B^{(e)})$ at $n_{0e} = 2 \times 10^{19} \text{ m}^{-3}$ is caused by resonance between frequencies of EPW and acoustic wave modified by the quantum correction term, i.e. $\omega_{pe}^2 \sim \omega_a^2 + k^2 V_{Fe}'^2$ (via δ_1^2) and the change of sign of $\text{Re}(\chi_B^{(e)})$ at $n_{0e} = 6 \times 10^{21} \text{ m}^{-3}$ is caused by resonance between frequencies of EPW and BSSM modified by the quantum correction term, i.e. $\omega_{pe}^2 \sim \omega_s^2 + k^2 V_{Fe}'^2$ (via δ_2^2).

Here, it should be pointed out that the resonance enhancement of Brillouin susceptibility is a common trend in semiconductor magneto plasmas. Singh et al.³² observed

switching between positively and negatively enhanced values of BSSM in piezoelectric semiconductor magneto plasmas by setting up resonance between frequencies of EPW and modified BSSM. Recently, Kumari et al. [11] observed switching between positively and negatively enhanced values of Brillouin susceptibility in semiconductor magneto plasmas by setting up resonance between frequency of coupled cyclotron-plasmon mode and Stokes mode. In the present case, by setting up resonances ($\omega_{pe}^2 \sim \omega_a^2 + k^2 V_{Fe}^2$ and $\omega_{pe}^2 \sim \omega_s^2 + k^2 V_{Fe}^2$), the negative and positive enhanced values of $\text{Re}(\chi_B^{(e)})$ can be obtained, which can be used for optical switching devices. In IISP, these resonances can be set up by proper selection of electron concentration. Around resonances $\text{Re}(\chi_B^{(e)})$ can be (positively or negatively) enhanced by one to two orders of magnitude.

Fig. 3 shows how the real part of the effective Brillouin susceptibility $\text{Re}(\chi_B^{(e)})$ varies with implanted colloid concentration n_{0d} for the cases: (i) in which QEs are excluded and (ii) in which QEs are included. To draw this behaviour, we consider the contribution of n_{0d} to $\text{Re}(\chi_B^{(e)})$; the contribution of n_{0e} to $\text{Re}(\chi_B^{(e)})$ is neglected. We consider the wide range of implanted colloid concentration ($10^2 \text{ m}^{-3} < n_{0d} < 10^6 \text{ m}^{-3}$). This clearly shows the substantial enhancement of $\text{Re}(\chi_B^{(e)})$ as well as change of its sign. For clear understanding, the features corresponding to both the cases can be explained separately.

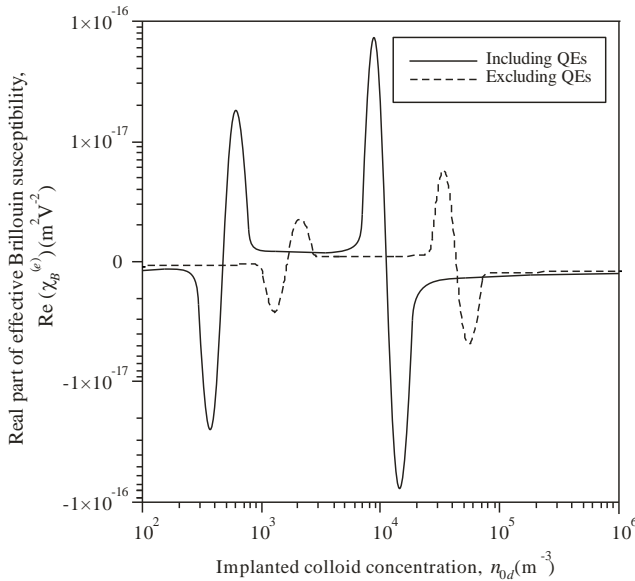


Fig. 3. Variation of real part of effective Brillouin susceptibility $\text{Re}(\chi_B^{(e)})$ with implanted colloid concentration n_{0d} for the cases: (i) excluding QEs, and (ii) including QEs

When QEs are not taken into account ($V_{Fd}' = 0$), $\text{Re}(\chi_B^{(e)})$ is negative, very small, and remain unaffected by the implanted colloid concentration for $n_{0d} \leq 9 \times 10^2 \text{ m}^{-3}$.

The regime $9 \times 10^2 \text{ m}^{-3} < n_{0d} \leq 3 \times 10^3 \text{ m}^{-3}$ is quite sensitive to the nature of curve. In this regime, with increasing n_{0d} , $\text{Re}(\chi_B^{(e)})$ starts decreasing, achieving a negative peak value ($-2.5 \times 10^{-18} \text{ m}^2 \text{ V}^{-2}$) at $n_{0d} = 1.4 \times 10^3 \text{ m}^{-3}$. Beyond this point, n_{0d} is only marginally increased, and $\text{Re}(\chi_B^{(e)})$ begins rapidly increasing. At $n_{0d} = 1.7 \times 10^3 \text{ m}^{-3}$, $\text{Re}(\chi_B^{(e)})$ vanishes. With further increasing n_{0d} beyond this value, $\text{Re}(\chi_B^{(e)})$ changes sign achieving a peak positive value ($2.5 \times 10^{-18} \text{ m}^2 \text{ V}^{-2}$) at $n_{0d} = 2 \times 10^3 \text{ m}^{-3}$. For $2 \times 10^3 \text{ m}^{-3} \leq n_{0d} \leq 3 \times 10^3 \text{ m}^{-3}$, $\text{Re}(\chi_B^{(e)})$ decreases sharply but remains positive and vanishingly small up to $n_{0d} < 2.5 \times 10^4 \text{ m}^{-3}$. The nature of curve of $\text{Re}(\chi_B^{(e)})$ versus n_{0d} is repeated again in the regime $2.5 \times 10^4 \text{ m}^{-3} \leq n_{0d} \leq 8 \times 10^4 \text{ m}^{-3}$ like the regime $9 \times 10^2 \text{ m}^{-3} < n_{0d} \leq 3 \times 10^3 \text{ m}^{-3}$. For $n_{0d} > 8 \times 10^4 \text{ m}^{-3}$, $\text{Re}(\chi_B^{(e)})$ continues to be negative and vanishingly small. The behaviour of $\text{Re}(\chi_B^{(e)})$ in the domain $9 \times 10^2 \text{ m}^{-3} < n_{0d} \leq 3 \times 10^3 \text{ m}^{-3}$ is caused by resonance between frequencies of dust plasma wave and acoustic wave, i.e. $\omega_{pd}^2 \sim \omega_a^2$ (via Δ^2) while the behaviour of $\text{Re}(\chi_B^{(e)})$ in the domain $2.5 \times 10^4 \text{ m}^{-3} \leq n_{0d} \leq 8 \times 10^4 \text{ m}^{-3}$ is caused by resonance between the frequencies of dust plasma wave and BSSM, i.e. $\omega_{pe}^2 \sim \omega_s^2$ (via Δ^2).

When QEs are taken into account ($V_{Fd}' \neq 0$), the entire spectrum has been shifted towards smaller values of colloid concentration and the peak (negative and positive values) of $\text{Re}(\chi_B^{(e)})$ have been enhanced significantly. The change of sign of $\text{Re}(\chi_B^{(e)})$ previously occurred at $n_{0d} = 1.7 \times 10^3$, and $4 \times 10^3 \text{ m}^{-3}$, have now been shifted to $n_{0d} = 5 \times 10^2$, and $1.1 \times 10^4 \text{ m}^{-3}$, respectively. This change occurred due to inclusion of QEs via appearance of the term $k^2 V_{Fd}'^2$ in Δ^2 . In this case, the change of sign of $\text{Re}(\chi_B^{(e)})$ at $n_{0d} = 1.7 \times 10^3 \text{ m}^{-3}$ is caused by resonance between frequencies of dust plasma wave and acoustic wave modified by the quantum correction term, i.e. $\omega_{pd}^2 \sim \omega_a^2 + k^2 V_{Fd}'^2$ and the change of sign of $\text{Re}(\chi_B^{(e)})$ at $n_{0d} = 4 \times 10^3 \text{ m}^{-3}$ is caused by resonance between frequencies of dust plasma wave and BSSM modified by the quantum correction term, i.e. $\omega_{pe}^2 \sim \omega_s^2 + k^2 V_{Fd}'^2$. In IISPs, these resonances can be set up by proper selection of implanted colloid concentration. Around resonances $\text{Re}(\chi_B^{(e)})$ can be (negatively or positively) enhanced by one to two orders of magnitude.

A comparison of $\text{Re}(\chi_B^{(e)}) - n_{0e}$ plot (Fig. 2) with $\text{Re}(\chi_B^{(e)}) - n_{0d}$ plot (Fig. 3) reveals that the behaviour of

$\text{Re}(\chi_B^{(e)})$ obtained by varying n_{0e} (from 10^{19} m^{-3} to 10^{23} m^{-3}) alone can be also obtained by varying n_{0d} (from 10^2 m^{-3} to 10^5 m^{-3}) but with inverted profile; the order of magnitudes of $\text{Re}(\chi_B^{(e)})$ in both cases being comparable. Thus, the present analysis offers one to choose doped semiconductors containing either electrons or implanted colloids or both to obtain (negative or positive) enhanced values of $\text{Re}(\chi_B^{(e)})$.

Fig. 4 shows how the real part of the effective Brillouin susceptibility $\text{Re}(\chi_B^{(e)})$ varies with pump field amplitude E_0 for the cases: (i) in which QEs are excluded and (ii) in which QEs are included. When QEs are negligible for $E_0 \leq 3 \times 10^7 \text{ Vm}^{-1}$, the curves corresponding to the two cases are closer and $\text{Re}(\chi_B^{(e)})$ show a linear variation with E_0 . However, QEs become significant for $E_0 > 3 \times 10^7 \text{ Vm}^{-1}$, the curves corresponding to the two cases gradually start deviating and $\text{Re}(\chi_B^{(e)})$ shows a parabolic variation with E_0 . For $E_0 \approx 10^8 \text{ Vm}^{-1}$, $\text{Re}(\chi_B^{(e)})$ ceases to increase with pump field amplitude. The result reveals that QEs on $\text{Re}(\chi_B^{(e)})$ in IISPs are dominating at higher pump fields.

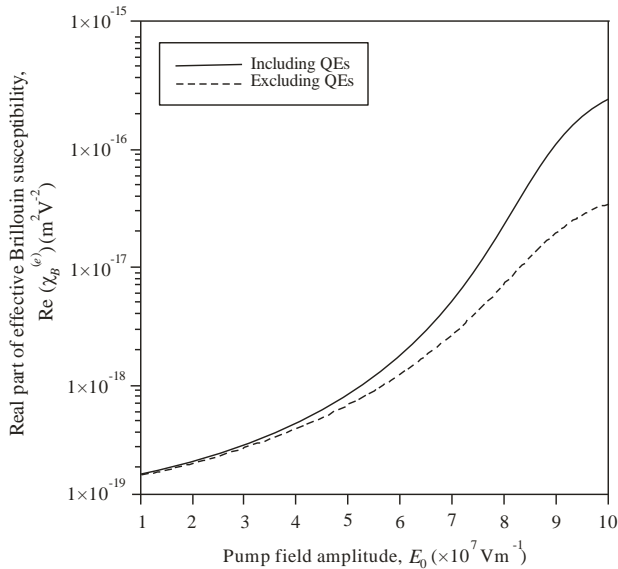


Fig. 4. Variation of real part of effective Brillouin susceptibility $\text{Re}(\chi_B^{(e)})$ with pump field amplitude E_0 for the cases: (i) excluding QEs, and (ii) including QEs

3.2. Threshold and gain characteristics of BSSM

Eqs. (22) and (23) can be used to study the nature of dependency of the threshold pump amplitude (E_{0T}) and the effective gain constant ($g_B^{(e)}$) of BSSM on several factors, including wave number magnitude (k), electron concentration (n_{0e}), and pump field amplitude (E_0). Figs. (5), (6), and (7) display the results.

Fig. 5 depicts the variation of threshold pump amplitude E_{0T} and effective gain constant $g_B^{(e)}$ of BSSM with wave number magnitude k for the cases: (i) excluding QEs, and (ii) including QEs.

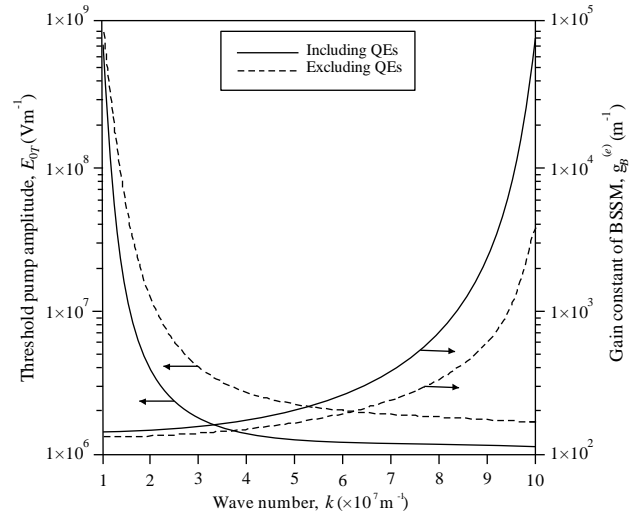


Fig. 5. Variation of threshold pump amplitude E_{0T} and effective gain constant $g_B^{(e)}$ of BSSM with wave number magnitude k for the cases: (i) excluding QEs, and (ii) including QEs

In both instances, we found that the nature of the curves is essentially the same; the difference is that when QEs are included, E_{0T} is significantly lower while $g_B^{(e)}$ is significantly greater than when they are excluded. The curves corresponding to both cases are extremely close to one another for smaller magnitudes of wave number ($\sim 10^7 \text{ m}^{-1}$), but they gradually diverge as wave number increases, showing that QEs on E_{0T} as well as $g_B^{(e)}$ are more pronounced at greater magnitudes of wave number. The threshold pump amplitude decreases very rapidly with wave number magnitude for $k < 3 \times 10^7 \text{ m}^{-1}$, the rate of fall decreases in the regime $3 \times 10^7 \text{ m}^{-1} \leq k \leq 5 \times 10^7 \text{ m}^{-1}$, and then becomes nearly independent for $k > 5 \times 10^7 \text{ m}^{-1}$. However, the effective gain constant of BSSM exhibits a linear variation with wave number magnitude for $k \leq 5 \times 10^7 \text{ m}^{-1}$ and then exhibit rapid increment for $k > 5 \times 10^7 \text{ m}^{-1}$. When QEs are not taken into account ($V_{Fe}' = 0$ and hence $\delta_2 = 0$), $E_{0T} \propto k^{-1}$ [Eq. (22)] and $g_B^{(e)} \propto k$ [Eq. (23)]. However, when QEs are taken into account, the term δ_1^2 containing k in Eq. (22) and the terms δ_1^2 and δ_2^2 containing k [Eq. (23)] get additionally modified and hence E_{0T} and $g_B^{(e)}$ exhibit the complex dependence on k .

Fig. 6 depicts the variation of threshold pump amplitude E_{0T} and effective gain constant $g_B^{(e)}$ of BSSM

with electron concentration n_{0e} for the cases: (i) excluding QEs), and (ii) including QEs.

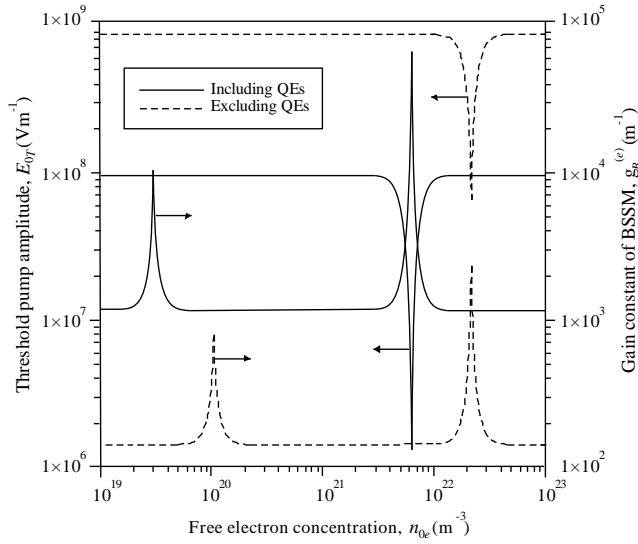


Fig. 6. Variation of threshold pump amplitude E_{OT} and effective gain constant $g_B^{(e)}$ of BSSM with electron concentration n_{0e} for the cases: (i) excluding QEs), and (ii) including QEs

When QEs are not taken account ($V_{Fe}' = 0$), E_{OT} is comparatively larger, remains independent of n_{0e} , except at $n_{0e} = 1.2 \times 10^{22} \text{ m}^{-3}$. However, $g_B^{(e)}$ is comparatively smaller, remains independent of n_{0e} , except at $n_{0e} = 1.1 \times 10^{20}$ and $1.2 \times 10^{22} \text{ m}^{-3}$. At $n_{0e} = 1.2 \times 10^{22} \text{ m}^{-3}$, E_{OT} exhibit minimization while $g_B^{(e)}$ exhibit sharp peak which is caused by resonance between frequencies of EPW and BSSM, i.e. $\omega_{pe}^2 \sim \omega_s^2$ (via δ_2^2). At $n_{0e} = 1.2 \times 10^{22} \text{ m}^{-3}$, $g_B^{(e)}$ exhibit another sharp peak which are caused by resonance between the frequencies of the EPW and the acoustic wave, i.e. $\omega_{pe}^2 \sim \omega_s^2$ (via δ_2^2). When QEs are taken into account ($V_{Fe}' \neq 0$), the plot's features are unaltered with the exception of the shifted peak value of the curve (at $n_{0e} = 2 \times 10^{19} \text{ m}^{-3}$ for E_{OT} and at $n_{0e} = 2 \times 10^{19}$ and $6 \times 10^{21} \text{ m}^{-3}$ for $g_B^{(e)}$) towards smaller values of electron concentration and E_{OT} has been decreased while $g_B^{(e)}$ has been increased significantly throughout the plotted regime of n_{0e} . This change occurred due to inclusion of QEs via appearance of the term $k^2 V_{Fe}'^2$ in δ_2^2 . In this case, the behaviour of E_{OT} is caused by resonance: $\omega_{pe}^2 \sim \omega_s^2 + k^2 V_{Fe}'^2$ (via δ_2^2) while the behaviour of $g_B^{(e)}$ is caused by resonances: $\omega_{pe}^2 \sim \omega_a^2 + k^2 V_{Fe}'^2$ (via δ_1^2) and $\omega_{pe}^2 \sim \omega_s^2 + k^2 V_{Fe}'^2$ (via δ_2^2). Thus, around resonance(s), the threshold pump amplitude

decreases while the effective gain constant of BSSM increases by one order of magnitude when QEs are excluded and two orders of magnitude when QEs are included.

It is important to note that the reduction of the threshold pump intensity necessary for SBS and the sharp peaks of Brillouin gain spectrum in magnetised semiconductor plasmas was achieved by Singh et al. [28] by establishing three resonances ($\bar{\omega}_p^2 \sim \omega_a^2$, $\bar{\omega}_p^2 \sim \omega_s^2$ and $\omega_c^2 \sim \omega_0^2$), under the cases: (i) excluding QEs, and (ii) including QEs. Moreover, they did not observe any shifting of minimization curves which inclusion of QEs. But in the present study, we obtained the minimization of threshold pump amplitude required for SBS in (unmagnetized) IISPs by setting up only a single resonance in each case, viz. $\omega_{pe}^2 \sim \omega_s^2$ (when QEs are excluded), and $\omega_{pe}^2 \sim \omega_s^2 + k^2 V_{Fe}'^2$ (when QEs are included) and the enhancement of gain constant of BSSM in (unmagnetized) IISPs by setting up only two resonances in each case, viz. $\omega_{pe}^2 \sim \omega_a^2$ and $\omega_{pe}^2 \sim \omega_s^2$ (when QEs are excluded), and $\omega_{pe}^2 \sim \omega_a^2 + k^2 V_{Fe}'^2$ and $\omega_{pe}^2 \sim \omega_s^2 + k^2 V_{Fe}'^2$ (when QEs are included). Also, we observed shifting of minimization/peak curves towards smaller values of electron concentration, which inclusion of QEs. This shifting may be advantageous in the development of widely tunable Brillouin oscillators.

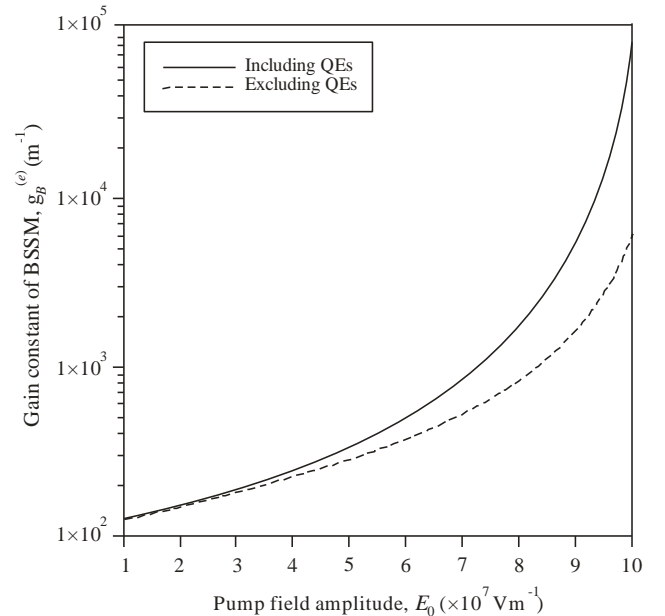


Fig. 7. Variation of effective gain constant $g_B^{(e)}$ of BSSM with pump field amplitude E_0 for the cases: (i) excluding QEs), and (ii) including QEs

Fig. 7 shows how the effective gain constant $g_B^{(e)}$ of BSSM varies with pump field amplitude E_0 for the

cases: (i) in which QEs are excluded and (ii) in which QEs are included. We noticed that $g_B^{(e)}$ exhibits curves of identical shape in both cases across the plotted range of E_0 . Both when QEs are excluded and when they are included, the curve has a parabola shape. When QEs are negligible for smaller values of E_0 ($\leq 3 \times 10^7 \text{ Vm}^{-1}$), the curves corresponding to both cases exactly overlap. The curves corresponding to both cases, however, begin to diverge with increasing E_0 ($> 3 \times 10^7 \text{ Vm}^{-1}$), which is the limit at which QEs become significant. This result is well in agreement with theoretical investigations of QEs on threshold and Brillouin gain characteristics of semiconductor magneto-plasmas [28]. This deviation of $g_B^{(e)}$ curves at large pump field amplitudes highlights the need to include QEs in SBS and the related phenomena.

4. Conclusions

In this paper, QEs on dispersion, threshold and gain characteristics of BSSM in IISPs are studied using QHD model. The dispersion characteristics of BSSM are strongly dependent on the electron as well as the implanted colloid concentration, whereas the threshold and gain characteristics of BSSM are dependent on electron concentration only. The numerical analysis is performed for n- InSb/CO₂ laser system for two different cases, viz. excluding QEs and including QEs. In both the cases, the analysis offers two achievable resonances ($\omega_{pe}^2 \sim \omega_a^2$ and $\omega_{pe}^2 \sim \omega_s^2$, when QEs are excluded, and $\omega_{pe}^2 \sim \omega_a^2 + k^2 V_{Fe}^2$ and $\omega_{pe}^2 \sim \omega_s^2 + k^2 V_{Fe}^2$, when QEs are included), at which the change of sign as well as an enhancement of real part of effective Brillouin susceptibility, minimization of threshold pump amplitude, and enhancement of effective Brillouin gain constant are obtained. The inclusion of QEs in the analysis shifts the entire spectrum towards smaller values of electrons (colloids) carrier concentration. In addition, the dispersion and gain characteristics of BSSM are insignificant for smaller pump field amplitudes ($\leq 3 \times 10^7 \text{ Vm}^{-1}$) and pronounced at higher pump field amplitudes ($> 3 \times 10^7 \text{ Vm}^{-1}$). As a result, the investigation improves our understanding of SBS processes in electron- and colloidal-based IISPs and establishes the suitability of the selected sample for the production of effective Brillouin amplifiers and tunable Brillouin lasers.

Acknowledgements

For many insightful suggestions, the authors are very grateful to Prof. M.R. Perrone, International Centre for Theoretical Physics, Italy and Prof. S.K. Ghoshal, Universiti Teknologi, Malaysia.

References

- [1] Z. Bai, H. Yuan, Z. Liu, P. Xu, Q. Gao, R. J. Williams, O. Kitzler, R. P. Mildren, Y. Wang, Z. Lu, *Optical Materials* **75**, 626 (2018).
- [2] S. Bhan, H. P. Singh, V. Kumar, M. Singh, *Optik* **184**, 464 (2019).
- [3] H. J. Kong, J. W. Yoon, D. H. Beak, J. S. Shin, S. K. Lee, D. W. Lee, *Laser Part. Beams* **25**, 225 (2007).
- [4] A. M. Scott, K. D. Ridley, *IEEE J. Quantum Electron.* **25**, 438 (1989).
- [5] X. Bao, Z. Zhou, Y. Wang, *Photonics* **2**, 14 (2021).
- [6] S. Mokkaapati, C. Jagadish, *Mat. Today* **12**, 22 (2009).
- [7] E. Garmire, *IEEE J. Select. Top. Quant. Electron.* **6**, 1094 (2000).
- [8] P. Kumari, B.S. Sharma, M. Singh, *Optik* **247**, 167878 (2021).
- [9] P. Kumari, B.S. Sharma, M. Singh, *Ind. J. Phys.* **96**, 3651 (2022).
- [10] Renu, Sanjay, M. Singh, *J. Opt.* **51**, 386 (2022).
- [11] P. Kumari, B.S. Sharma, M. Singh, *Pramana J. Phys.* **96**, 49 (2022).
- [12] A. Kumar, S. Dahiya, N. Singh, M. Singh, *J. Optoelectron. Adv. M.* **24**, 125 (2022).
- [13] A. Kumar, S. Dahiya, N. Singh, M. Singh, *J. Nonlin. Opt. Phys. Mater.* **30**, 2150010 (2021).
- [14] J. Kennedy, J. Leveneur, G. V. M. Williams, D. R. G. Mitchell, *Nanotech.* **22**, 115602 (2011).
- [15] D. Kumar, S. Gupta, T. Jin, R. Nongjai, A. Kandasami, S.N. Piramanayagam, *IEEE Magnet. Lett.* **9**, 4500305 (2017).
- [16] W. C. Jung, *Trans. Elect. Electron. Mater.* **11**, 120 (2010).
- [17] M. Salimullah, Z. Ehsan, K. Zubia, H. A. Shah, G. Murtaza, *J. Appl. Phys.* **102**, 053301 (2007).
- [18] I. Zeba, C. Uzma, M. Jamil, M. Salimullah, P. K. Shukla, *Phys. Plasmas* **17**, 032105 (2010).
- [19] S. Ghosh, P. Khare, *Ind. J. Pure Appl. Phys.* **44**, 183 (2006).
- [20] N. Yadav, S. Ghosh, P. S. Malviya, *Chin. Phys. B* **26**, 015203 (2017).
- [21] S. Ghosh, P. Khare, *Eur. Phys. J. D* **35**, 521 (2005).
- [22] S. K. Ghosh, P. Thakur, *Eur. Phys. J. D* **37**, 417 (2006).
- [23] P. K. Shukla, S. Ali, *Phys. Plasmas* **12**, 114502 (2005).
- [24] F. Hass, *Phys. Plasmas* **12**, 062117 (2005).
- [25] D. Singh, B. S. Sharma, M. Singh, *Materials Today: Proc.* **49**, 1383 (2022).
- [26] D. Singh, B. S. Sharma, M. Singh, *Iran. J. Sci. Technol. Trans. Sci.* **46**, 999 (2022).
- [27] D. Singh, B. S. Sharma, M. Singh, *J. Nonlin. Opt. Phys. Mater.* **31**, 235009 (2022).
- [28] D. Singh, B. S. Shrama, M. Singh, *J. Opt.* **51**, 969 (2022).
- [29] Pravesh, S. Dahiya, D. Singh, M. Singh, *Pramana J. Phys.* **97**, 58 (2023).
- [30] J. Singh, S. Dahiya, M. Singh, *J. Opt.* **51**, 317 (2021).
- [31] T. Ferdous, M. Salahuddin, M. R. Amin,

- M. Salimullah, Phys. Rev. B **52**, 9044 (1995).
- [32] S. Dubey, S. Ghosh, Phys. Rev. B **49**, 5246 (1994).
- [33] F. Haas, L. G. Garcia, J. Goedert, G. Manfredi, Phys. Plasmas **10**, 3858 (2003).
- [34] M. Singh, P. Aghamkar, N. Kishore, P. K. Sen, Opt. Laser Tech. **40**, 215 (2008).
- [35] J. Gahlawat, M. Singh, S. Dahiya, J. Optoelectron. Adv. M. **23**(3-4), 183 (2021).
- [36] Gopal, B. S. Sharma, M. Singh, J. Optoelectron. Adv. M. **24**(11-12), 584 (2022).

*Corresponding author: msgur_18@yahoo.com